Simple spike dynamics of Purkinje cells in the macaque vestibulo-cerebellum during passive whole-body self-motion

Jean Laurens[a] and Dora E. Angelaki[a,b,c,1]

[a]Department of Neuroscience, Baylor College of Medicine, Houston, TX 77056; [b]Center for Neural Science, New York University, New York, NY 10003; and [c]Tandon School of Engineering, New York University, New York, NY 10003

Contributed by Dora E. Angelaki, November 20, 2019 (sent for review September 12, 2019; reviewed by Stefan Glasauer and Clément Léna)

Theories of cerebellar functions posit that the cerebellum implements internal models for online correction of motor actions and sensory estimation. As an example of such computations, an internal model resolves a sensory ambiguity where the peripheral otolith organs in the inner ear sense both head tilts and translations. Here we exploit the response dynamics of two functionally coupled Purkinje cell types in the vestibular part of the caudal vermis (lobules IX and X) to understand their role in this computation. We find that one population encodes tilt velocity, whereas the other, translation-selective, population encodes linear acceleration. We predict that an intermediate neuronal type should temporally integrate the output of tilt-selective cells into a tilt position signal.

internal model | cerebellum | vestibular

More than a century since the pioneering work of Ramon y Cajal (1), the cerebellum continues to represent a powerful model for understanding neural circuits. Its stereotyped anatomy (2), its remarkably organized connectivity (3, 4), and its profoundly tractable cellular identities (5, 6) have motivated numerous recent advances in dissecting how cerebellar circuits are wired using modern molecular and optogenetic manipulations (7–12). In parallel to superb cellular and circuit organization discoveries, theory-driven studies have defined algorithmic computations likely performed by the cerebellar circuit. These computations extend beyond motor learning, into a modular organization for sensorimotor prediction and internal models (13–20).

One such internal model implemented by brainstem–cerebellar circuits merges signals from both vestibular end organs, the otoliths and semicircular canals, to resolve a sensory ambiguity (Fig. 1*A*) (21): otolith afferents cannot distinguish linear acceleration (A) experienced during translations from gravitational acceleration (G) experienced during head tilt. Instead, otolith afferents encode the total gravito-inertial acceleration (GIA) = G + A (Fig. 1*B*), thus responding identically to translational acceleration and tilt position (units are m/s^2, or equivalently, degrees of tilt). Theoretical (22–33) and experimental (34–43) studies have demonstrated that the brain resolves this ambiguity by using head rotation signals, originating from the vestibular semicircular canals, to track head movements relative to vertical, from which the gravitational component (G) can be estimated.

Although mathematical models of tilt–translation discrimination somewhat differ in their formulation (22–33), they all incorporate two salient computations (Fig. 1*C*): 1) the activity of semicircular canals, which encodes rotation velocity in an egocentric (head) reference frame (units are °/s), is spatially transformed [equation 1 in Fig. 1*C*; the vectorial cross-product converts head-referenced rotation velocity signal (Ω) into a gravity referenced tilt velocity signal, dG/dt] and 2) this canal-driven tilt velocity signal must combine with otolith afferent information, but the latter signals linear acceleration or tilt position relative to gravity. Often it has been assumed that the canal-driven, spatially transformed signal must be temporally integrated (equation 2 in Fig. 1*C*; integration of tilt velocity signals into position) in order to estimate G, which is then subtracted from the otolith signal to compute linear acceleration (equation 3 in Fig. 1*C*). Note, however, that the brain might implement alternative but functionally equivalent computational schemes. In particular, equation 3 in Fig. 1*C* could be implemented in the velocity domain (equation 3′ in Fig. 1*D*), implying a differentiation of the otolith-driven signal rather than an integration of the canal-driven signal.

Laurens et al. (41) have indeed identified translation-selective and tilt-selective Purkinje cells as the neuronal correlates of the hypothesized tilt and translation signals. They have demonstrated that tilt-selective Purkinje cells encode spatially transformed signals (i.e., equation 1 in Fig. 1*C* or downstream) and that tilt- and translation-selective cells are functionally coupled: when the GIA is constant, they observed that the activity of tilt- and translation-selective cells were inversely correlated, as implied by equation 3 or equation 3′ in Fig. 1 *C* and *D*.

However, the sinusoidal stimuli used in past experiments cannot resolve neuronal response dynamics, because these neurons do not follow minimum-phase linear system predictions (44, 45). Therefore, whether tilt-selective neurons encode tilt (G) or tilt velocity (abbreviated here as dG) and whether translation-selective Purkinje cells encode linear acceleration (A) or its derivative (abbreviated here as dA) is unknown. Distinguishing between these possibilities is a crucial step for understanding the computational algorithms implemented by central vestibular regions.

In this study, we consider three alternative hypotheses, all of which would be consistent with the hypothesized computations: tilt-selective cells may encode dG and translation-selective cells A (hypothesis H_1, Fig. 1*E*). If this holds, then there is a functional need for temporal integration of the simple-spike signal of

Significance

This study characterizes the response dynamics of two types of Purkinje neurons in the vestibulo-cerebellum that are known to encode head motion. We find that one type encodes tilt velocity, whereas the other encodes linear acceleration. We compare these results to current theories that posit that the cerebellum implements internal models for sensing head motion and discuss the role of tilt- and translation-selective cells in the theoretical sequence of computations.

Author contributions: D.E.A. designed research; J.L. analyzed data; and J.L. and D.E.A. wrote the paper.

Reviewers: S.G., Brandenburg University of Technology; and C.L., École Normale Supérieure Paris.

The authors declare no competing interest.

Data deposition: Data supporting the study's conclusion are available in the following repository: https://github.com/JeanLaurens/PNAS-2019.

[1]To whom correspondence may be addressed. Email: da93@nyu.edu.

This article contains supporting information online at https://www.pnas.org/lookup/suppl/doi:10.1073/pnas.1915873117/-/DCSupplemental.

First published January 27, 2020.

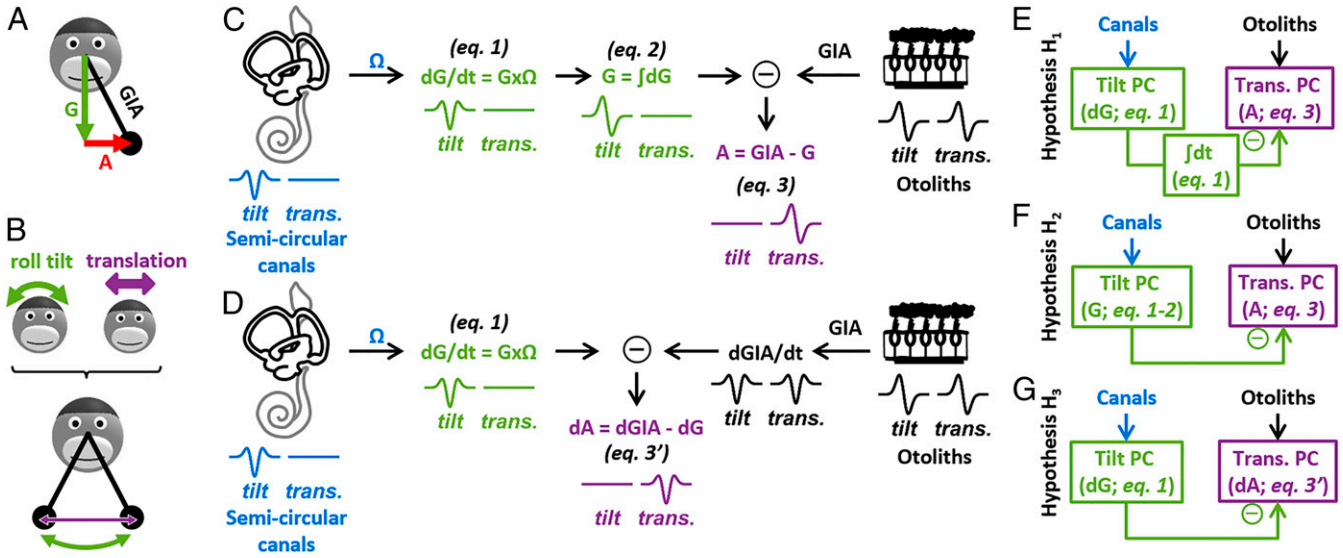

Fig. 1. Internal model of head motion for resolving the tilt/translation ambiguity. (*A*) Illustration of the gravito-inertial force vector (GIA) sensed by the otoliths, which is the sum of gravitational (G) and inertial (A) acceleration. (*B*) Illustration of the GIA during tilt and translation: both follow approximately the same trajectory (note that the trajectory of the GIA is circular during tilt [green], resulting in a small upward stimulation of the otoliths that can be neglected for small motion angles). Thus, the otoliths detect both stimuli but do not discriminate them. (*C*) Simplified model of tilt/translation discrimination (from ref. 30). Angular velocity (Ω) is sensed by the semicircular canals and used to track the gravitational component (G) of the GIA (equations 1 and 2), which allows extracting the linear acceleration component by subtraction (equation 3). See text for details. The temporal waveforms shown are further detailed in *SI Appendix*, Fig. S1, which shows a decomposition of the motion stimuli into dynamic components. (*D*) Alternative architecture for tilt/translation discrimination that operates in the derivative domain (see text). (*E*–*G*) Hypotheses (H_1, H_2, and H_3) of how internal model variables are represented in simple spike responses. Hypothesis H_1 assumes that tilt-selective Purkinje cells encode the output of equation 1 in *C*, hypothesis H_2 assumes that tilt-selective Purkinje cells encode the output of equation 2 in *C*, and hypothesis H_3 assumes that the cerebellum implements the computations shown in *D*.

tilt-selective cells to implement equation 2 in Fig. 1*C*, before it reaches translation-selective cells (equation 3 in Fig. 1*C*). This would suggest that another, yet unidentified, cell type, may encode a tilt signal (G). Alternatively, tilt-selective cells may encode G and translation-selective cells A (hypothesis H_2, Fig. 1*F*). In this case, the integration (equation 2 in Fig. 1*C*) would occur upstream of tilt-selective Purkinje cells or possibly in their dendritic tree. Finally, tilt-selective cells may encode dG and translation-selective cells dA (hypothesis H_3, Fig. 1*G*), in which case the need for equation 2 in Fig. 1*C* would be eliminated from the cerebellar circuitry that distinguishes tilt from translation (although it would still have to be implemented, possibly in a separate stage, in order to provide the term G in equation 1 in Fig. 1*C*).

To distinguish among these three hypotheses, we have recorded Purkinje cell simple spike (SS) activity using transient tilt, translation, and tilt–translation stimuli that allow quantitative assessment of the response dynamics of tilt- and translation-selective Purkinje cells. A transient stimulus approach is necessary as sinusoidal stimuli cannot resolve complex dynamics that do not follow linear systems properties (44–46). The present results strongly support hypothesis H_1, consistent with the notion that Purkinje cell SS activity reflects sensory prediction errors.

Results

Experimental Findings. We recorded from Purkinje cells in the caudal vermis (lobules IX and X) of macaque monkeys during transient tilt and translation stimuli with biphasic linear acceleration and Gaussian linear velocity profiles (σ = 250 ms), as illustrated in Fig. 2 *A*–*E* (47). The tilt and translation stimuli were matched such that they activated the otoliths identically (Fig. 2*E*, first/second column) (35–41). During tilt–translation motion, tilt-driven and translation-driven otolith activation cancel each other (Fig. 2*E*, third column). Because the derivative of the biphasic tilt position (Fig. 2*B*, green) and linear acceleration (Fig. 2*C*, magenta) profiles follow a triphasic curve (e.g., tilt velocity in Fig. 2*D*, blue) and because these signals ride on top of a large spontaneous activity, the multiple temporal components of the models in Fig. 1*C* (i.e., G, A, GIA, and dG) as well as additional dynamic components (i.e., the integral of G and A or the second derivative of G and A; *SI Appendix*, Fig. S1*A*) can be distinguished.

Typical responses of tilt-selective and translation-selective Purkinje cells during the transient stimuli (with σ = 250 ms) are illustrated in Fig. 2 *F* and *G*. During tilt, the example tilt cell exhibited a triphasic response modulation, with a peak to trough amplitude of 28 spk/s, that was either proportional (preferred direction, PD; Fig. 2 *F*, *Top*) or inversely proportional (anti-PD; Fig. 2 *F*, *Bottom*) to tilt velocity (Fig. 2*D*, blue). Here PD is defined as the direction along which firing rate is positively correlated with the stimulus; therefore, the cell is inhibited during motion in its PD because tilt velocity is negative (Fig. 2*D*). The example tilt cell's response resembles tilt velocity (the large peak/trough responses to tilt are flanked by smaller troughs/peaks) not only during tilt but also during tilt–translation (Fig. 2 *F*, *Left* and *Right* columns, respectively) but is negligible during translation (Fig. 2 *F*, *Middle* column). By contrast, the example translation cell modulates little during tilt (Fig. 2 *G*, *Left*) but responds vigorously to translation (Fig. 2 *G*, *Middle*) and tilt–translation (Fig. 2 *G*, *Right*). During translation along the cell's PD (Fig. 2 *G*, *Top*), the cell exhibits a biphasic response with a peak to trough amplitude of 94 spk/s, whose dynamics follows the acceleration stimulus (Fig. 2*C*, magenta). The response reverses during motion along the anti-PD (Fig. 2 *G*, *Bottom*). Note that both tilt and translation Purkinje cells modulate during tilt–translation, when only the canals are dynamically modulated. This illustrates the fact that NU Purkinje cells receive convergent inputs from both sensors (37, 41).

These two example cells suggest that tilt Purkinje cells may follow tilt velocity (dG), whereas translation Purkinje cells may follow linear acceleration (A), in support of hypothesis H_1. We analyzed the transient responses of 30 NU Purkinje cells (three macaques) which were specifically selected to be either

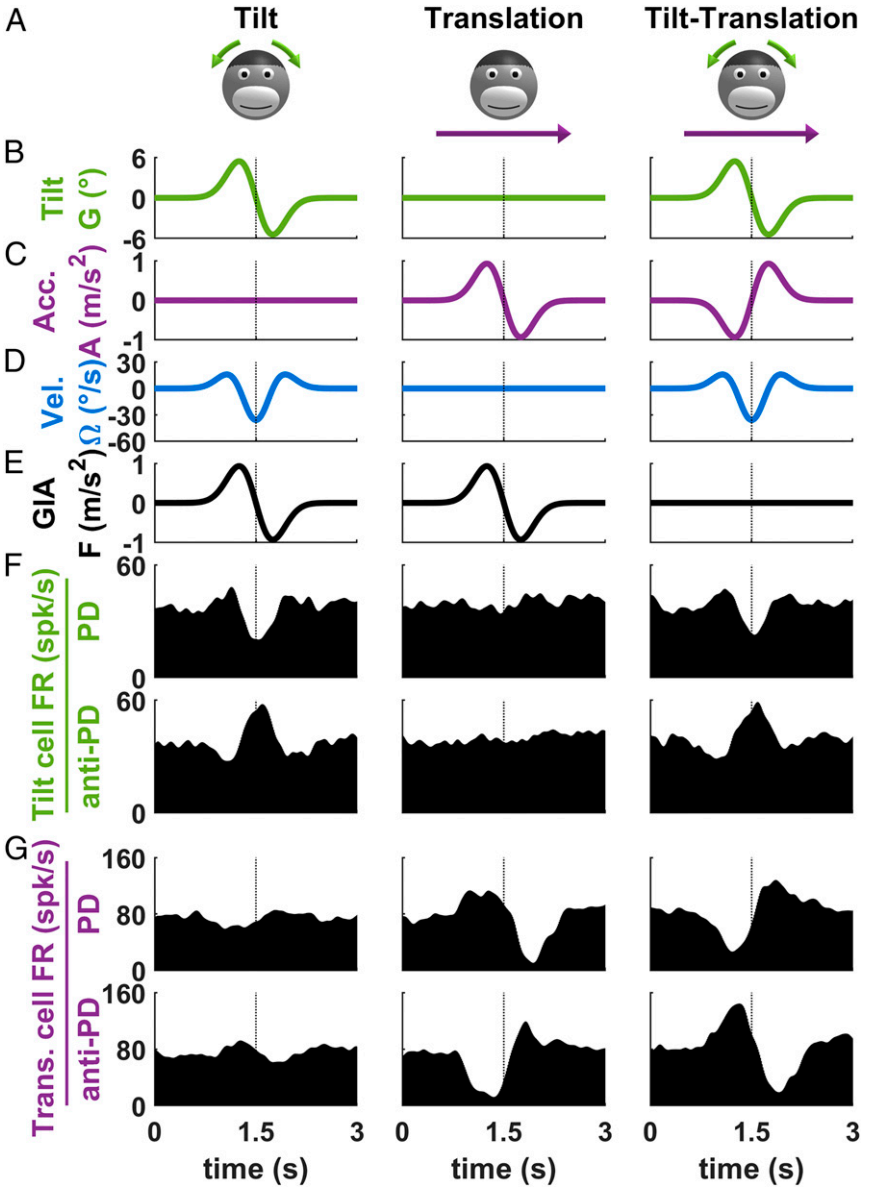

Fig. 2. Example tilt- and translation-selective Purkinje cell responses during tilt, translation, and tilt–translation. (*A*) Illustration of the motion stimuli. (*B* and *C*) Temporal profiles of the gravitational (i.e., tilt; *B*) and translational acceleration (*C*) component of the motion stimuli. (*D* and *E*) Temporal profiles of the physical variables sensed by the vestibular system: the tilt velocity (*D*) is detected by the semicircular canals, and the GIA (*E*) is detected by the otoliths. (*F* and *G*) Firing rate (FR) of a tilt-selective and translation-selective Purkinje cell. *Upper* and *Lower* rows display the neuronal responses in the preferred direction (PD) and in the opposite direction (anti-PD), respectively. The PD is defined as the direction along which tilt-selective neurons increase their firing in response to positive tilt velocity and translation-selective neurons increase their firing in response to positive acceleration. Data are shown in response to transient stimuli with $\sigma = 250$ ms.

tilt-selective ($n = 14$) or translation-selective ($n = 16$) following the criteria of (40, 41). Note that cell classification was similar using transient and sinusoidal stimuli (*SI Appendix*, Table S1).

We evaluated neuronal modulation by computing the difference in firing rate between motion in the PD and anti-PD and dividing by two (Fig. 3). Note that this process cancels a quantitatively smaller omnidirectional component (*SI Appendix*, Fig. S2) and only focuses on the direction-dependent responses. We measured each neuron's peak-to-trough direction-dependent response during tilt and translation, as illustrated in the scatterplot of Fig. 3*A*. During translation, the responses of translation-selective cells were one order of magnitude larger than those of tilt-selective cells (38.9 spk/s, CI = [26.5 to 57.2] versus 3.9 spk/s, CI = [2.8 to 5.4]; $P = 4.10^{-6}$, geometric mean and Wilcoxon sign rank test). In contrast, tilt- and translation-selective cells had comparable peak-to-trough modulation during tilt (tilt-selective cells, 15.1 spk/s, CI = [12.2 to 18.7]; translation-selective cells, 13.2 spk/s, CI = [9.4 to 18.4], $P = 0.55$). Thus, the range of response modulation amplitude during transient tilt and translation was remarkably similar to previous findings using sinusoidal stimuli (41).

Next we assessed which dynamic components are represented in neural responses. Our working hypotheses (H_1, H_2, and H_3) consider only two temporal components: 1) G (tilt position) and A (linear acceleration), both of which have identical waveforms (Fig. 1 and see also *SI Appendix*, Fig. S1), and 2) dG (tilt velocity) and dA (derivative of linear acceleration; i.e., jerk) signals, both of which also have identical waveforms (Fig. 1 and see also

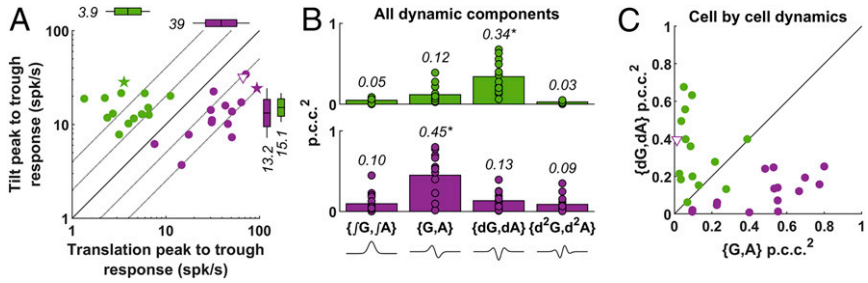

Fig. 3. Dynamic response components of tilt (green) and translation (magenta) Purkinje cells. (*A*) Scatterplot of peak-to-trough response amplitude (in spk/s) during tilt and translation. The box and whisker plots indicate geometric mean (center of boxes), 95% confidence intervals of the mean (boxes), and SD of the population (whiskers). The example cells in Fig. 2 are represented by stars. One translation-selective cell with atypical dynamics is marked by a triangle. (*B*) Squared partial coefficients of correlation of the $\int$G,$\int$A; G,A; dG,dA; and d^2G,d^2A components (whose waveforms are illustrated at the bottom) in tilt (*Upper*; green) and translation Purkinje cells (*Lower*; magenta). Dots indicate individual cells, and bars indicate population average. (*C*) Comparison of the squared partial correlation coefficients of biphasic (G,A) and triphasic (dG,dA) response components in tilt- and translation-selective Purkinje cells. Note that this analysis is agnostic to whether the cell encodes tilt or translation (because the G profile during tilt matches exactly the A profile during translation). Yet, it gives different answers for the two cell types, suggesting different dynamics. Data are shown in response to transient stimuli with $\sigma = 250$ ms. All analyses are based on direction-dependent responses; summary of omnidirectional modulation responses is shown in *SI Appendix*, Fig. S2.

SI Appendix, Fig. S1). To characterize the cells' response dynamics independently of their selectivity for tilt, translation, or mixture thereof, we grouped motion variables with similar dynamics (i.e., G with A and dG with dA) and computed the squared partial coefficient of correlation of each pair (G,A and dG,dA) for each individual cell's response. For generality, we included two additional dynamic components ($\int$G,$\int$A and d^2G,d^2A; *SI Appendix*, Fig. S1) in the analysis. We found that the dG,dA component had the highest contribution to the responses of tilt cells (Fig. 3*B*; $P < 0.01$, multiple paired Wilcoxon tests, Bonferroni correction), whereas the G,A component had the highest contribution in translation cells (Fig. 3*B*; $P < 0.01$, multiple paired Wilcoxon tests, Bonferroni correction). In contrast, the squared partial correlation coefficients of the $\int$G,$\int$A and d^2G,d^2A components were minimal. Thus, only the dG, dA, G, and A components are considered in further analysis.

When plotted on a cell-by-cell basis, we found that the two cell types showed distinctly different response dynamics (Fig. 3*C*, green vs. magenta). Many tilt-selective cells clustered along the ordinate, and most (12/14, $P = 0.002$, paired Wilcoxon test) appear above the diagonal, indicating that the dG,dA profile dominates the responses of tilt-selective Purkinje cells. Considering that based on ref. 41, tilt cells encode tilt-related signals and not simply canal-related signals (Ω), we conclude that tilt-selective cells carry predominantly a tilt velocity (dG) signal. Translation-selective cells clustered close to the abscissa, and only one cell appeared above the diagonal ($P = 0.0016$), indicating that translation-selective cells carry acceleration (A) signals.

These conclusions are further illustrated in the average response profiles (Fig. 4; see also individual cell responses in *SI Appendix*, Fig. S3). In line with the example cells in Fig. 2*F*, the average translation-selective cell exhibited a biphasic response profile that followed linear acceleration (Fig. 4*C*, magenta). The average tilt-selective cell exhibited a triphasic response profile that followed tilt velocity (Fig. 4*C*, green), although it displayed a slight asymmetry, where the second excitatory peak was attenuated compared to the first. This can be attributed to a small, but nonzero, G response, as shown in Fig. 4 *D–F*. We plotted the G response component of tilt cells (Fig. 4*D*) as a function of their dG component. We found that both were correlated ($P < 10^{-3}$, bootstrap test), indicating that tilt-selective cells carry a G response component that is proportional to the dG component with about half the amplitude (slope = 0.47, CI = [0.27 to 0.79]). Plotting the average dG and G response components together (Fig. 4*E*) illustrates that the first peak of the G component (gray) tends to increase the first peak of the dG component (black), whereas the second peak of the G component reduces the last peak of the dG component. When these components are added (Fig. 4*F*, broken black line), this results in an asymmetrical profile that matches the average response profile of tilt cells (Fig. 4*F*, green, same as in Fig. 4*C*). This analysis, which reveals that tilt-selective cells encode primarily dG but also carry a weaker G component, is compatible with previous observations during sinusoidal motion at 0.5 Hz (41) where the response lagged tilt velocity by 36° (i.e., shifted toward tilt position). We repeated the same analysis for translation-selective cells (Fig. 4 *G–I*). We found that these cells carry a small dA response (slope = −0.16, CI = [−0.24 to −0.06], $P = 10^{-3}$), although this component was too small to alter the cell's biphasic response profile markedly (Fig. 4*H*). In agreement, we observed (41) that the response phase of translation-selective cells was closely aligned with linear acceleration during sinusoidal motion. Note that the average peak–valley response amplitude of tilt- and translation-selective cells during tilt are identical in Fig. 3*A*. However, after averaging the response profiles across all cells, the population of translation-selective cells exhibits a smaller modulation than that of tilt-selective cells (Fig. 4 *C*, *Left*, green versus magenta). This indicates that the response profiles of individual translation-selective cells are more variable and tend to average each other out at the population level.

Analyses of responses to a longer transient stimulus ($\sigma = 500$ ms) gave identical results (*SI Appendix*, Fig. S4). In fact, other than a small but systematic increase in the gain of tilt cells (*SI Appendix*, Fig. S4 *E* and *F*), both sets of transient stimuli yield identical results.

Discussion

We have shown that tilt- and translation-selective Purkinje cells differ in response dynamics: tilt-selective cells encode primarily tilt velocity, whereas translation-selective cells encode linear acceleration. Laurens et al. (41) have shown that tilt-selective Purkinje cells in the nodulus and uvula encode tilt signals, i.e., spatially transformed rotation signals corresponding to equation 1 in Fig. 1*C* or downstream). Using stimuli where the GIA is constant, they also showed the population response amplitudes of tilt and translation-selective are inversely correlated. Furthermore, local gabazine injection into the cortex converts translation-selective Purkinje cells into GIA-coding cells (48). Thus, it has been proposed that tilt signals encoded by tilt-selective cells are subtracted from net otolith signals (GIA) to compute a head translation signal encoded by translation-selective Purkinje cells (41), as predicted by the internal model

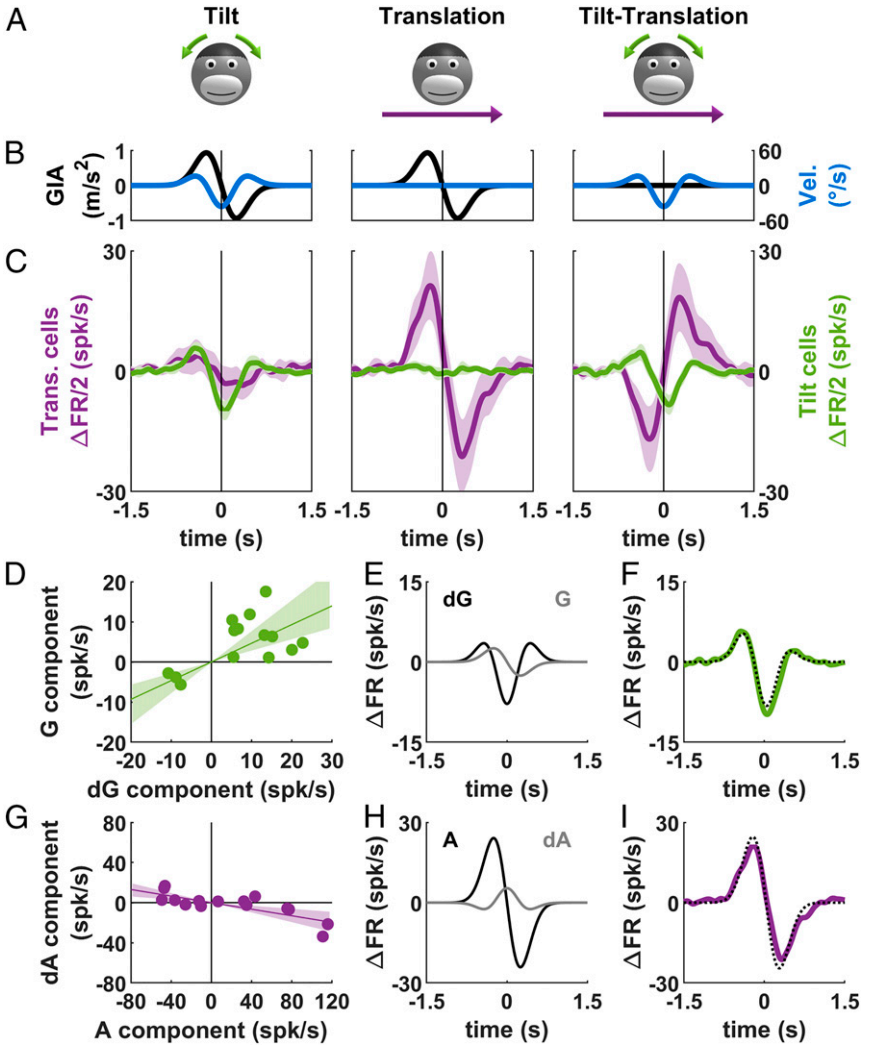

Fig. 4. Average response profiles of tilt- and translation-selective cells. (*A* and *B*) Illustration of the stimuli (*A*) and sensory inputs (*B*), as in Fig. 2 (all individual cells are shown in *SI Appendix*, Fig. S3). (*C*) Average direction-dependent response ΔFR (*Materials and Methods*) of tilt-selective (green; right ordinate axis) and translation-selective (magenta; left ordinate axis) cells. The bands represent 95% CIs. Data are shown in response to transient stimuli with $\sigma = 250$ ms. Summary of neuronal responses during transient motion of longer duration is shown in *SI Appendix*, Fig. S4. (*D*) Correlation between the dG and G response components (defined as a signed peak to trough response amplitude; *SI Materials and Methods*, *Composite Model*) of tilt-selective cells. (*E*) Average dG (black) and G (gray) response components of tilt-selective cells (*SI Materials and Methods*, *Composite Model*). (*F*) Comparison between the sum of the dG and G components in *E* and the average response of tilt-selective cells in *C*. (*G–I*) Analysis of the A and dA responses of translation-selective cells, as in *D–F*. The translation-selective cell with atypical dynamic in Fig. 3 is excluded.

framework. However, the dynamic aspects of this computation had not been resolved by previous studies. Combined with the present findings, we conclude that the output of tilt Purkinje cells should be temporally integrated before relayed to translation-selective Purkinje cells.

The discrimination of tilt and translation stimuli is one of the best studied computations in the vestibular system (34–41, 49) and has been instrumental in revealing internal model computations in the vestibulo-cerebellum. Gravitational acceleration associated with head tilt and linear acceleration caused by translations are physically indistinguishable (21). Both are sensed by regular and irregular otolith afferents that differ in their response dynamics (50) but provide identical information about tilt and translation occurring at similar frequencies. Since the range of natural tilt and translational motion overlap widely (51, 52), simply filtering otolith signals cannot segregate natural tilt and translations, with the exception of static otolith stimuli that are, by default, interpreted as tilt (53). Thus, accurate self-motion sensing requires the disambiguation process described in this study.

The framework of internal models has been the dominant theory of vestibular processing in the past decades (22–33) and is closely related to the framework used to model motor control and adaptation (54–62). Initially supported by behavioral studies using passive motion stimuli (34, 63–65), the implementation of internal models in central vestibular pathways has been confirmed by neurophysiological experiments of tilt/translation discrimination (35–43) and active head movements (66–72).

Laurens and Angelaki (31) have formulated a Kalman filter to model neuronal responses in the vestibular nuclei, cerebellar cortex and deep cerebellar nuclei during both active and passive motion. This model postulates that the brain constructs internal estimate of head motion that are used to predict vestibular sensory inflow. When the predicted sensory signals do not match actual sensory afference, the resulting sensory prediction errors are transformed into Kalman feedback signals that update the internal estimate of head motion. Importantly, when the head is

moved passively, then these feedback pathways implement the sequence of computations in Fig. 1*C* and ref. 31. It is notable that the feedback signals predicted by the Kalman filter model match the dynamics of tilt- and translation-selective cells. Specifically, the Kalman feedback that updates the internal estimate of tilt (G) is a tilt velocity signal (figure 5 in ref. 31), whereas the Kalman feedback that updates the internal estimate of translation (A) is a linear acceleration signal (figure 6 in ref. 31). This finding supports the hypothesis that the SS activity of Purkinje cells carries feedback signals derived from sensory prediction errors, a critical component of a dynamical control framework supporting optimal sensorimotor functions (15–20, 73, 74). The Kalman filter also predicts that feedback signals, and consequently the activity of tilt- and translation-selective cells, should be profoundly attenuated during active tilt and translation, similar to neuronal responses measured in the vestibular nuclei, fastigial nuclei, and cerebellar cortex (42, 66, 67, 67–71, 75). In agreement with this prediction, one study (75) conducted when rats learn to balance on a swing indicates that Purkinje cells in various lobules (V to X) of the cerebellar vermis encode tilt velocity during external perturbations but not learned active movement.

Although tilt-selective Purkinje cells encode predominantly tilt velocity, we found that they carry a smaller but consistent tilt position component (Fig. 4 *D*–*F*). This finding is consistent with Laurens et al. (41), which reported response phase shifted on average by 36° toward tilt position during sinusoidal tilt at 0.5 Hz. Thus, tilt-selective Purkinje cells may themselves be within the dynamic system that generates the tilt position signal, although their responses remain closer to tilt velocity than position.

In a separate study (46), we have demonstrated that vestibular and fastigial nuclei neurons that respond to translation often encode combinations of linear velocity, acceleration, and jerk. Interestingly, we found that the velocity and jerk components were characterized by large spatial modulation offset, that corresponds to the omnidirectional modulation described here. In contrast, the linear acceleration component exhibited cosine spatial tuning, that corresponds to the directional modulation described here. The response of translation-selective Purkinje cells reported here matches this pattern: we found that their directional response predominantly encodes linear acceleration, whereas their omnidirectional response reflects linear velocity (*SI Appendix*, Fig. S2). While the directional component of translation-selective cells matches the linear acceleration signal postulated to underlie internal model computations, the omnidirectional component may serve distinct but yet undetermined functions.

Collectively, these results imply that the output of tilt-selective Purkinje cells is subtracted from an otolithic signal upstream of translation-selective Purkinje cells or in their dendritic tree. This subtraction may be realized by an inhibitory circuit between tilt- and translation-selective cells with equivalent preferred directions (e.g., cells that are activated by leftward tilt and rightward acceleration). Alternatively, this operation may be realized by an excitatory circuit between tilt- and translation-selective cells with opposite preferred direction.

Future studies may determine which neural pathway transmits tilt-selective cells output back onto translation-selective Purkinje cells. A salient question is whether this neuronal feedback loop is implemented outside of the cerebellar cortex, i.e., in through fastigial and/or vestibular nuclei neurons. Translation-selective cells have been identified in the vestibular nuclei (35, 69), and fastigial nuclei (35, 36). A recent study (76) proposed that some cells in the deep fastigial nuclei encode dynamic gravity signals. However, this study did not test whether these cells encode tilt velocity relative to gravity (dG), as opposed to rotation velocity in an egocentric reference frame (Ω), which is sensed by the canals and encoded by the fastigial nuclei (72). It is notable that many neurons in the fastigial nuclei encode combinations of canal and dynamic otolith signals (77–80) or spatially transformed rotation and translation signals (e.g., in a body-referenced frame; refs. 70, 72, and 81–83). Therefore, because it was never quantitatively tested, it remains unknown whether fastigial neurons encode dynamic gravity signals. Nevertheless, since these vertical rotation responses followed velocity, what is clear is that they do not encode G. Instead, it is possible that the G signal is contributed to the cerebellum through the vestibular nuclei, where G signals have been reported previously (84). Thus, G signals could reach translation-selective Purkinje cells (that would implement equation 3 in Fig. 1*C*) through mossy fiber projections from the vestibular nuclei.

Nevertheless, the most parsimonious possibility is that the entire process of tilt/translation discrimination occurs in the cerebellar cortex. For instance, Purkinje axon collaterals onto the cerebellar cortex (10, 12, 85) may allow the temporal integration (equation 2 in Fig. 1*C*) to occur through granular layer interneurons, e.g., unipolar brush cells (UBCs) and/or granule/Golgi cells. These cells may in turn provide G signals to translation-selective cells, who would implement equation 3 in Fig. 1*C*.

Materials and Methods

Three male rhesus Macaques, aged 3, 4, and 9 y, were used in the study. Experimental procedures were in accordance with US National Institutes of Health guidelines and approved by the Animal Studies Committee at Washington University in St. Louis (approval 20100230) and Baylor College of Medicine (protocol AN-5795). Primates were installed in a three-axis rotator mounted on a linear sled (Acutronics Inc.). Purkinje cells in lobules X and IX of the caudal vermis were recorded extracellularly using epoxy-coated tungsten microelectrodes (5 or 20 MΩ impedance; FHC). Transient motion profiles were generated by computing the derivative of a Gaussian function with SD σ = 250 ms, resulting in a biphasic signal that was scaled to an amplitude of ±5.6° to generate the tilt position stimulus and ±0.93 m/s^2 to generate the linear acceleration stimulus. A tilt–translation stimulus was created by applying tilt and translation stimuli simultaneously so that the resultant gravito-inertial acceleration was null. Neuronal responses were analyzed using multiple linear regression, and statistical tests were based on bootstrap procedures. Details of the experiment procedures, data analysis, and modeling are provided in *SI Appendix*, *SI Methods*. Data supporting the study's conclusion are available in the following repository: https://github.com/JeanLaurens/PNAS-2019.

ACKNOWLEDGMENTS. This work was supported by NIH grant DC004260. We acknowledge Hui Meng's contributions to the recordings.

1. S. Ramon y Cajal, Histologie du Système Nerveux de l'homme et des Vertébrés (Maloine, Paris, 1911), vol. 2, pp. 153–173.
2. S. L. Palay, V. Chan-Palay, "A guide to the synaptic analysis of the neuropil" in *Cold Spring Harbor Symposia on Quantitative Biology*, N. Ford, Ed. (Cold Spring Harbor Laboratory Press, 1976), pp. 1–16.
3. T. J. H. Ruigrok, Ins and outs of cerebellar modules. *Cerebellum* **10**, 464–474 (2011).
4. J. Voogd, Cerebellar zones: A personal history. *Cerebellum* **10**, 334–350 (2011).
5. J. Eccles, Functional meaning of the patterns of synaptic connections in the cerebellum. *Perspect. Biol. Med.* **8**, 289–310 (1965).
6. J. C. Eccles, The cerebellum as a computer: Patterns in space and time. *J. Physiol.* **229**, 1–32 (1973).
7. L. Ankri *et al.*, A novel inhibitory nucleo-cortical circuit controls cerebellar Golgi cell activity. *Elife* **4**, e06262 (2015).
8. Z. Gao *et al.*, Excitatory cerebellar nucleocortical circuit provides internal amplification during associative conditioning. *Neuron* **89**, 645–657 (2016).
9. C. C. Guo, M. C. Ke, J. L. Raymond, Cerebellar encoding of multiple candidate error cues in the service of motor learning. *J. Neurosci.* **34**, 9880–9890 (2014).
10. C. Guo *et al.*, Purkinje cells directly inhibit granule cells in specialized regions of the cerebellar cortex. *Neuron* **91**, 1330–1341 (2016).
11. T. D. B. Nguyen-Vu *et al.*, Cerebellar Purkinje cell activity drives motor learning. *Nat. Neurosci.* **16**, 1734–1736 (2013).
12. L. Witter, S. Rudolph, R. T. Pressler, S. I. Lahlaf, W. G. Regehr, Purkinje cell collaterals enable output signals from the cerebellar cortex to feed back to Purkinje cells and interneurons. *Neuron* **91**, 312–319 (2016).
13. D. M. Wolpert, R. C. Miall, M. Kawato, Internal models in the cerebellum. *Trends Cogn. Sci.* **2**, 338–347 (1998).

14. A. M. Green, D. E. Angelaki, Multisensory integration: Resolving sensory ambiguities to build novel representations. *Curr. Opin. Neurobiol.* **20**, 353–360 (2010).
15. R. Shadmehr, M. A. Smith, J. W. Krakauer, Error correction, sensory prediction, and adaptation in motor control. *Annu. Rev. Neurosci.* **33**, 89–108 (2010).
16. L. S. Popa, A. L. Hewitt, T. J. Ebner, Predictive and feedback performance errors are signaled in the simple spike discharge of individual Purkinje cells. *J. Neurosci.* **32**, 15345–15358 (2012).
17. D. Popa *et al*., Functional role of the cerebellum in gamma-band synchronization of the sensory and motor cortices. *J. Neurosci.* **33**, 6552–6556 (2013).
18. L. S. Popa, M. L. Streng, A. L. Hewitt, T. J. Ebner, The errors of our ways: Understanding error representations in cerebellar-dependent motor learning. *Cerebellum* **15**, 93–103 (2016).
19. L. S. Popa, M. L. Streng, T. J. Ebner, Long-term predictive and feedback encoding of motor signals in the simple spike discharge of Purkinje cells. *eNeuro* **4**, ENEURO.0036-17.2017 (2017).
20. M. L. Streng, L. S. Popa, T. J. Ebner, Modulation of sensory prediction error in Purkinje cells during visual feedback manipulations. *Nat. Commun.* **9**, 1099 (2018).
21. A. Einstein, *Über Das Relativitätsprinzip und Die aus Demselben Gezogenen Folgerungen* (Jahrbuch der Radioaktivität und Elektronik, 1907), vol. IV, p. 454.
22. R. Mayne, "A systems concept of the vestibular organs" in *Vestibular System Part 2: Psychophysics, Applied Aspects and General Interpretations*, H. H. Kornhuber, Ed. (Springer, 1974), pp. 493–580.
23. C. M. Oman, A heuristic mathematical model for the dynamics of sensory conflict and motion sickness hearing in classical musicians. *Acta Otolaryngol.* **94**, 4–44 (1982).
24. J. Borah, L. R. Young, R. E. Curry, Optimal estimator model for human spatial orientation. *Ann. N. Y. Acad. Sci.* **545**, 51–73 (1988).
25. D. M. Merfeld, Modeling the vestibulo-ocular reflex of the squirrel monkey during eccentric rotation and roll tilt. *Exp. Brain Res.* **106**, 123–134 (1995).
26. S. Glasauer, D. M. Merfeld, "Modelling three-dimensional vestibular responses during complex motion stimulation" *Three-Dimensional Kinematics of Eye, Head and Limb Movements*, M. Fetter, T. Haslwanter, H. Misslich, D. Tweed, Eds. (Hardwood Academic Publishers, Reading, UK, 1997), pp. 387–398.
27. J. E. Bos, W. Bles, Theoretical considerations on canal-otolith interaction and an observer model. *Biol. Cybern.* **86**, 191–207 (2002).
28. L. H. Zupan, D. M. Merfeld, C. Darlot, Using sensory weighting to model the influence of canal, otolith and visual cues on spatial orientation and eye movements. *Biol. Cybern.* **86**, 209–230 (2002).
29. J. Laurens, J. Droulez, Bayesian processing of vestibular information. *Biol. Cybern.* **96**, 389–404 (2007).
30. J. Laurens, D. E. Angelaki, The functional significance of velocity storage and its dependence on gravity. *Exp. Brain Res.* **210**, 407–422 (2011).
31. J. Laurens, D. E. Angelaki, A unified internal model theory to resolve the paradox of active versus passive self-motion sensation. *Elife* **6**, e28074 (2017).
32. F. Karmali, D. M. Merfeld, A distributed, dynamic, parallel computational model: The role of noise in velocity storage. *J. Neurophysiol.* **108**, 390–405 (2012).
33. K. Lim, F. Karmali, K. Nicoucar, D. M. Merfeld, Perceptual precision of passive body tilt is consistent with statistically optimal cue integration. *J. Neurophysiol.* **117**, 2037–2052 (2017).
34. D. M. Merfeld, L. Zupan, R. J. Peterka, Humans use internal models to estimate gravity and linear acceleration. *Nature* **398**, 615–618 (1999).
35. D. E. Angelaki, A. G. Shaikh, A. M. Green, J. D. Dickman, Neurons compute internal models of the physical laws of motion. *Nature* **430**, 560–564 (2004).
36. A. G. Shaikh *et al*., Sensory convergence solves a motion ambiguity problem. *Curr. Biol.* **15**, 1657–1662 (2005).
37. T. A. Yakusheva *et al*., Purkinje cells in posterior cerebellar vermis encode motion in an inertial reference frame. *Neuron* **54**, 973–985 (2007).
38. T. Yakusheva, P. M. Blazquez, D. E. Angelaki, Frequency-selective coding of translation and tilt in macaque cerebellar nodulus and uvula. *J. Neurosci.* **28**, 9997–10009 (2008).
39. T. Yakusheva, P. M. Blazquez, D. E. Angelaki, Relationship between complex and simple spike activity in macaque caudal vermis during three-dimensional vestibular stimulation. *J. Neurosci.* **30**, 8111–8126 (2010).
40. J. Laurens, H. Meng, D. E. Angelaki, Computation of linear acceleration through an internal model in the macaque cerebellum. *Nat. Neurosci.* **16**, 1701–1708 (2013).
41. J. Laurens, H. Meng, D. E. Angelaki, Neural representation of orientation relative to gravity in the macaque cerebellum. *Neuron* **80**, 1508–1518 (2013).
42. G. P. Dugué, M. Tihy, B. Gourévitch, C. Léna, Cerebellar re-encoding of self-generated head movements. *Elife* **6**, e26179 (2017).
43. T. L. Stay, J. Laurens, R. V. Sillitoe, D. E. Angelaki, Genetically eliminating Purkinje neuron GABAergic neurotransmission increases their response gain to vestibular motion. *Proc. Natl. Acad. Sci. U.S.A.* **116**, 3245–3250 (2019).
44. D. E. Angelaki, J. D. Dickman, Spatiotemporal processing of linear acceleration: Primary afferent and central vestibular neuron responses. *J. Neurophysiol.* **84**, 2113–2132 (2000).
45. J. D. Dickman, D. E. Angelaki, Vestibular convergence patterns in vestibular nuclei neurons of alert primates. *J. Neurophysiol.* **88**, 3518–3533 (2002).
46. J. Laurens *et al*., Transformation of spatiotemporal dynamics in the macaque vestibular system from otolith afferents to cortex. *Elife* **6**, e20787 (2017).
47. J. Laurens, D. E. Angelaki, Simple spike dynamics of Purkinje cells in Macaques. GitHub. https://github.com/JeanLaurens/PNAS-2019. Deposited 20 November 2019.
48. T. A. Yakusheva, D. E. Angelaki, P. M. Blazquez, Inactivation of GABA-B receptors in the cerebellar nodulus and uvula changes vestibular responses of Purkinje cells (abstract). *eNeuro*, Program No. 164.09/MM1 (2013).
49. D. E. Angelaki, M. Q. McHenry, J. D. Dickman, S. D. Newlands, B. J. M. Hess, Computation of inertial motion: Neural strategies to resolve ambiguous otolith information. *J. Neurosci.* **19**, 316–327 (1999).
50. M. Jamali, J. Carriot, M. J. Chacron, K. E. Cullen, Coding strategies in the otolith system differ for translational head motion vs. static orientation relative to gravity. *Elife* **8**, e45573 (2019).
51. J. Carriot, M. Jamali, M. J. Chacron, K. E. Cullen, The statistics of the vestibular input experienced during natural self-motion differ between rodents and primates. *J. Physiol.* **595**, 2751–2766 (2017).
52. J. Carriot, M. Jamali, K. E. Cullen, M. J. Chacron, Envelope statistics of self-motion signals experienced by human subjects during everyday activities: Implications for vestibular processing. *PLoS One* **12**, e0178664 (2017).
53. A. Graybiel, Oculogravic illusion. *AMA Arch. Opthalmol.* **48**, 605–615 (1952).
54. D. M. Wolpert, Z. Ghahramani, M. I. Jordan, An internal model for sensorimotor integration. *Science* **269**, 1880–1882 (1995).
55. K. P. Körding, D. M. Wolpert, Bayesian integration in sensorimotor learning. *Nature* **427**, 244–247 (2004).
56. E. Todorov, Optimality principles in sensorimotor control. *Nat. Neurosci.* **7**, 907–915 (2004).
57. H. Chen-Harris, W. M. Joiner, V. Ethier, D. S. Zee, R. Shadmehr, Adaptive control of saccades via internal feedback. *J. Neurosci.* **28**, 2804–2813 (2008).
58. M. Berniker, M. Voss, K. Körding, Learning priors for Bayesian computations in the nervous system. *PLoS One* **5**, e12686 (2010).
59. M. Berniker, K. Körding, Bayesian approaches to sensory integration for motor control. *Wiley Interdiscip. Rev. Cogn. Sci.* **2**, 419–428 (2011).
60. D. W. Franklin, D. M. Wolpert, Computational mechanisms of sensorimotor control. *Neuron* **72**, 425–442 (2011).
61. M. Sağlam, N. Lehnen, S. Glasauer, Optimal control of natural eye-head movements minimizes the impact of noise. *J. Neurosci.* **31**, 16185–16193 (2011).
62. M. Sağlam, S. Glasauer, N. Lehnen, Vestibular and cerebellar contribution to gaze optimality. *Brain* **137**, 1080–1094 (2014).
63. D. M. Merfeld, L. R. Young, G. D. Paige, D. L. Tomko, Three dimensional eye movements of squirrel monkeys following postrotatory tilt. *J. Vestib. Res.* **3**, 123–139 (1993).
64. J. Laurens, D. Straumann, B. J. M. Hess, Processing of angular motion and gravity information through an internal model. *J. Neurophysiol.* **104**, 1370–1381 (2010).
65. J. Laurens, D. Strauman, B. J. Hess, Spinning versus wobbling: How the brain solves a geometry problem. *J. Neurosci.* **31**, 8093–8101 (2011).
66. J. E. Roy, K. E. Cullen, Dissociating self-generated from passively applied head motion: Neural mechanisms in the vestibular nuclei. *J. Neurosci.* **24**, 2102–2111 (2004).
67. K. E. Cullen, J. X. Brooks, M. Jamali, J. Carriot, C. Massot, Internal models of self-motion: Computations that suppress vestibular reafference in early vestibular processing. *Exp. Brain Res.* **210**, 377–388 (2011).
68. K. E. Cullen, The vestibular system: Multimodal integration and encoding of self-motion for motor control. *Trends Neurosci.* **35**, 185–196 (2012).
69. J. Carriot, J. X. Brooks, K. E. Cullen, Multimodal integration of self-motion cues in the vestibular system: Active versus passive translations. *J. Neurosci.* **33**, 19555–19566 (2013).
70. J. X. Brooks, K. E. Cullen, The primate cerebellum selectively encodes unexpected self-motion. *Curr. Biol.* **23**, 947–955 (2013).
71. J. X. Brooks, K. E. Cullen, Early vestibular processing does not discriminate active from passive self-motion if there is a discrepancy between predicted and actual proprioceptive feedback. *J. Neurophysiol.* **111**, 2465–2478 (2014).
72. J. X. Brooks, J. Carriot, K. E. Cullen, Learning to expect the unexpected: Rapid updating in primate cerebellum during voluntary self-motion. *Nat. Neurosci.* **18**, 1310–1317 (2015).
73. S. G. Lisberger, Physiologic basis for motor learning in the vestibulo-ocular reflex. *Otolaryngol. Head Neck Surg.* **119**, 43–48 (1998).
74. A. Kennedy *et al*., A temporal basis for predicting the sensory consequences of motor commands in an electric fish. *Nat. Neurosci.* **17**, 416–422 (2014).
75. R. X. Lee, J.-J. Huang, C. Huang, M.-L. Tsai, C.-T. Yen, Plasticity of cerebellar Purkinje cells in behavioral training of body balance control. *Front. Syst. Neurosci.* **9**, 113 (2015).
76. I. Mackrous, J. Carriot, M. Jamali, K. E. Cullen, Cerebellar prediction of the dynamic sensory consequences of gravity. *Curr. Biol.* **29**, 2698–2710.e4 (2019).
77. C. Siebold, L. Glonti, S. Glasauer, U. Büttner, Rostral fastigial nucleus activity in the alert monkey during three-dimensional passive head movements. *J. Neurophysiol.* **77**, 1432–1446 (1997).
78. C. Siebold *et al*., Canal-otolith interaction in the fastigial nucleus of the alert monkey. *Exp. Brain Res.* **136**, 169–178 (2001).
79. A. Wilden, S. Glasauer, J. F. Kleine, U. Büttner, Modelling transfer characteristics of vestibular neurons in the fastigial nucleus of the behaving monkey on the basis of canal-otolith interaction. *Neuroreport* **13**, 799–804 (2002).
80. U. Büttner *et al*., Multimodal signal integration in vestibular neurons of the primate fastigial nucleus. *Ann. N. Y. Acad. Sci.* **1004**, 241–251 (2003).
81. J. F. Kleine *et al*., Trunk position influences vestibular responses of fastigial nucleus neurons in the alert monkey. *J. Neurophysiol.* **91**, 2090–2100 (2004).
82. J. X. Brooks, K. E. Cullen, Multimodal integration in rostral fastigial nucleus provides an estimate of body movement. *J. Neurosci.* **29**, 10499–10511 (2009).
83. C. Z. Martin, J. X. Brooks, A. M. Green, Role of rostral fastigial neurons in encoding a body-centered representation of translation in three dimensions. *J. Neurosci.* **38**, 3584–3602 (2018).
84. W. Zhou, B. F. Tang, S. D. Newlands, W. M. King, Responses of monkey vestibular-only neurons to translation and angular rotation. *J. Neurophysiol.* **96**, 2915–2930 (2006).
85. J. C. Eccles, M. Ito, J. Szentágothai, Eds., "The axon collaterals of Purkinje cells" in *The Cerebellum as a Neuronal Machine* (Springer, 1967), pp. 178–187.